Peripapillary Choroidal Vascularity Index and Microstructure of Parapapillary Atrophy

Min Hee Suh,[1] Jun Woo Park,[1] Neha Khandelwal,[2–4] and Rupesh Agrawal[2–4]

[1]Department of Ophthalmology, Haeundae Paik Hospital, Inje University College of Medicine, Busan, South Korea
[2]National Healthcare Group Eye Institute, Department of Ophthalmology, Tan Tock Seng Hospital, Singapore, Singapore
[3]Singapore Eye Research Institute, Singapore National Eye Center, Singapore, Singapore
[4]School of Material Science and Engineering, Nanyang Technological University, Singapore, Singapore

Correspondence: Min Hee Suh, Department of Ophthalmology, Haeundae Paik Hospital, Inje University College of Medicine, 1435 Jwa-dong, Haeundae-gu, Busan 612-030, Korea; crishuna6@gmail.com.

Submitted: November 29, 2018
Accepted: August 7, 2019

Citation: Suh MH, Park JW, Khandelwal N, Agrawal R. Peripapillary choroidal vascularity index and microstructure of parapapillary atrophy. *Invest Ophthalmol Vis Sci*. 2019;60:3768–3775. https://doi.org/10.1167/iovs.18-26286

Purpose. To investigate the association between the microstructure of β-zone parapapillary atrophy (βPPA) and choroidal vascularity index (CVI) determined by spectral-domain optical coherence tomography (SD-OCT) in glaucomatous eyes.

Methods. A total of 160 eyes of 160 primary open-angle glaucoma patients with βPPA were included. Total choroidal area (TCA), luminal area (LA), and CVI were measured at a 3.5-mm distance from the Bruch's membrane (BM) opening center by image binarization of SD-OCT B-scans. The widths of βPPA with BM (βPPA_{+BM}) and without BM (βPPA_{-BM}), and juxtapapillary choroidal thickness (JPCT) were measured on six radial SD-OCT images. OCT angiography–derived parapapillary deep-layer microvasculature dropout (MvD_P) was also derived.

Results. In the multivariate regression analysis, larger βPPA_{+BM} was significantly associated with smaller TCA and smaller LA ($P < 0.05$, respectively), but not with CVI and JPCT ($P > 0.05$, respectively). Meanwhile, βPPA_{-BM} was not significantly associated with TCA, LA, CVI, or JPCT in the multivariate regression analysis ($P > 0.05$).

Conclusions. Despite significant relationship between the choroidal thinning and larger βPPA_{+BM}, choroidal vascularity was not associated with the βPPA_{+BM} width. These findings suggest that the presumed common pathogenic mechanism between RPE atrophy and peripapillary choroidal thinning may not be mediated by the impaired choroidal perfusion in glaucomatous eyes. Future studies on the mechanisms in explaining the relationship between the atrophy of retinal pigment epithelium (RPE) and choroid in glaucoma are needed.

Keywords: choroidal vascularity index, OCT, CVI, parapapillary atrophy, JPCT

The choroid is a highly vascularized structure that is known to be associated with the pathophysiology of various ocular diseases.[1–5] Although the peripapillary choroidal vasculature does not supply the anterior optic nerve directly, it shares the common origin of perfusion, short posterior ciliary artery, with the juxtacanalicular posterior ciliary arterioles that supply the laminar and immediate retrolaminar tissue and that pass through the scleral flange where the loading of IOP is greatest.[6–10] In addition, juxtacanalicular choroidal circulation is more susceptible to acute IOP elevation in the monkey eye than the posterior and peripheral chordal circulation.[11] Therefore, it has been suggested that reduced choroidal vasculature may play a role in the pathogenesis of glaucoma.[12,13] Recent studies have found that reduced volume of juxtapapillary choroid was associated with β-zone parapapillary atrophy (βPPA) in glaucomatous eyes, and suggested that vascular compromise derived by retinal pigment epithelium (RPE) and juxtapapillary choroidal atrophy is the main mechanism of βPPA.[14,15] However, it is also possible that decreased choroidal vasculature is an epiphenomenon of the choroidal atrophy that was directly associated with the βPPA.[14] Previous studies are limited in elucidating this issue because they used choroidal thickness as a surrogate for the choroidal vasculature.[14–16] Assessment of the relationship between the βPPA and choroidal vasculature after adjusting the influence of the choroidal structure is needed.

Recently, in vivo quantification of the choroidal vasculature by image binarization of spectral-domain optical coherence tomography (SD-OCT) was introduced.[2–5,17–20] Particularly, our recent study found that SD-OCT–derived choroidal vascularity index (CVI) measured outside the βPPA was reduced in eyes with OCT angiography (OCT-A)–derived parapapillary deep-layer microvasculature damage within the βPPA.[20]

Therefore, the purpose of the present study was to assess the relationship between parapapillary choroidal vascularity measured by image binarization of SD-OCT and the microstructure of βPPA.

Methods

This study included primary open-angle glaucoma (POAG) patients who had visited the Haeundae Paik Hospital Glaucoma Clinic between January 2017 and April 2018. It was approved by the Institutional Review Board of Haeundae Paik Hospital and all procedures conformed to the tenets of the Declaration of Helsinki. Informed consent was obtained from each participant.

Study Subjects

All of the participants underwent an ophthalmic examination, including measurement of best-corrected visual acuity (BCVA), refraction, slit-lamp biomicroscopy, intraocular pressure (IOP) measurement by Goldmann applanation tonometry, gonioscopy, central corneal thickness (CCT) measurement with the Pentacam Scheimpflug imaging system (Oculus Optikgeräte GmbH, Wetzlar, Germany), axial length (AXL) measurement by IOL Master (Carl Zeiss Meditec, Dublin, CA, USA), dilated fundus examination, simultaneous color and red-free fundus photography (TRC-NW8; Topcon, Tokyo, Japan), standard automated perimetry (SAP) (Humphrey Field Analyzer; 30-2 Swedish interactive threshold algorithm; Carl Zeiss Meditec), SD-OCT, and OCT-A (Spectralis; Heidelberg Engineering GmbH, Heidelberg, Germany).[20,21] The SAP and all of the imaging tests were performed within a 6-month period.[21] Systolic and diastolic blood pressures (BPs) were measured at the height of the heart using an automatic BP monitor (Model Easy X 800 [R/L]; JAWON Medical Co. Ltd., Kyungsan, Korea). Mean arterial pressure was calculated as one-third systolic BP + two-thirds diastolic BP, and mean ocular perfusion pressure (MOPP) as the difference between two-thirds of the mean arterial pressure and the IOP.[22] An optic disc hemorrhage (DH) was defined as an isolated flame-shaped or splinter hemorrhage on the optic nerve head (ONH) based on regular optic disc examinations or standardized review of fundus photographs performed approximately every 6 months.[20,21]

The inclusion criteria were visible βPPA of a temporal width $\geq$ 100 μm on fundus photographs of at least one radial scan measured by the built-in caliper of SD-OCT, and BCVA $\geq$ 20/40.[22] The exclusion criteria were a history of ocular surgery (except for uneventful cataract or glaucoma surgery), intraocular diseases other than glaucoma (e.g., diabetic retinopathy or nonglaucomatous optic neuropathy), or systemic diseases (e.g., stroke or pituitary tumor) that could influence the study results, and unreliable visual field (VF) or poor-quality imaging tests.[22]

POAG was defined as the presence of open angles on gonioscopy, and glaucomatous optic nerve damage (i.e., focal thinning, notching, localized or diffuse atrophy of the retinal nerve fiber layer [RNFL]), and compatible repeated VF defect.[20] A glaucomatous VF defect was defined as a VF outside the normal limits on the glaucoma hemifield test or a pattern standard deviation outside 95% normal limits as confirmed on two consecutive, reliable ($\leq$33% fixation losses and false negatives, $\leq$15% false positives) tests.[22]

If both eyes of a subject were eligible for the study, one of the eyes was selected randomly.

Dropout of Deep-Layer Microvasculature in Parapapillary Atrophy

Details on the Spectralis OCT-A and determination of the parapapillary deep-layer microvasculature are available elsewhere.[20–22] The 15° × 10° scan pattern of the OCT-A Module incorporated into the OCT2 platform provides for noninvasive visualization of the vasculature by averaging five rapid repeats of 256 B-scans. This technology has an acquisition speed of 85 kHz, a central wavelength of 880 nm, and lateral and axial resolutions of 5.7 and 3.9 μm per pixel, respectively. Based on a review by two interpreters (M.H.S. and J.W.P.), OCT-A images judged to be of poor quality according to the following criteria were excluded: (1) quality score <25; (2) poor clarity; (3) residual motion artifacts visible as irregular vessel pattern or disc boundary on en face angiogram; (4) local weak signal; and (5) choroidal-layer segmentation errors.[21–23] Two independent observers (M.H.S. and J.W.P.) masked to the patients' optic disc features and other characteristics determined parapapillary deep-layer microvasculature dropout (MvD_P) as complete dropout of the choriocapillaris or microvasculature contained in the scleral flange within the βPPA on both horizontal and en face OCT-A vessel-density maps. MvD_P was required to be present on at least four consecutive horizontal B-scans and to be $\geq$200 μm in diameter on at least one scan.[20,22,24] Discrepancies between the two interpreters were resolved by consensus, or, if consensus could not be reached, the subject was excluded from the analysis.[22]

Spectral-Domain Optical Coherence Tomography Imaging

Spectralis OCT2 Glaucoma Module Premium Edition (GMPE) software (version 1.9.17.0) (Spectralis; Heidelberg Engineering GmbH) provides 24 consecutive radial B-scans and an ONH Radial Circle (RC) scan pattern that are aligned according to the fovea-to-Bruch's membrane (BM) opening center axis. This scan pattern was used to determine the βPPA microstructure, BM opening area, fovea–BM opening angle, TCA, CVI, and RNFL thicknesses calculated at each point on a set-diameter (3.5 mm) circle in a global area.[20,22] Juxtapapillary choroidal thickness (JPCT) and focal LC defect were determined by using the 20° × 20° high-resolution scan pattern that includes 48 radial B-scans in the enhanced depth imaging (EDI) mode. Focal LC defects defined as laminar disinsertions or laminar holes violating the normal U- or W-shaped contour of the anterior laminar surface were determined by two masked independent observers (M.H.S. and H.R.K.), and subjects on whom the two observers failed to reach consensus were excluded.[20,25–27] The mean JPCT, defined as the choroidal area within 500 μm of the border tissue of Elsching, was calculated as the average of values measured by masked observers (J.W.P. and H.R.K.) using the built-in manual drawing tool of the Spectralis viewer software 24 meridians from the 12 radial B-scan images of 20° × 20° EDI Spectralis SD-OCT.[16]

Measurement of β-Zone Parapapillary Atrophy

The PPA region was evaluated using the Spectralis viewer, which facilitated synchronous viewing of the selected location on the OCT image and the color-converted infrared fundus image.[28–31] The β-zone PPA was subdivided into βPPA_{+BM} and βPPA_{-BM}. βPPA_{+BM} was defined as an area between the tips of the RPE and BM, and βPPA_{-BM} as an exposed border tissue between the clinical disc margin and the BM opening (Figs. 1A1-2, 1B1-2).[28–32] Clinical disc margin was defined as an innermost clinically visible hyperreflective border on both the infrared fundus images and OCT. The temporal widths of βPPA_{+BM} and βPPA_{-BM} were measured at six radial scans of which the center was located at the fovea-to-BM opening center axis. If the temporal margin of the ONH or βPPA was not well visualized, adjacent radial scans 15° apart were used for the measurement. The presence and width of βPPA, βPPA_{+BM}, and βPPA_{-BM} were measured independently by two experienced observers (J.W.P. and H.R.K.) masked to patients' clinical information, using the built-in caliper tool of Spectralis SD-OCT. Discrepancies between the two interpreters were resolved by consensus, or, if consensus could not be reached, the subject was excluded from the analysis. The averages of the two examiners were used in the final analysis.

Measurement of Choroidal Vascularity Index and Total Choroidal Area

Details on the measurement of TCA and CVI using the 3.5-mm-sized ONH-RC scan of the Spectralis OCT2 GMPE software are

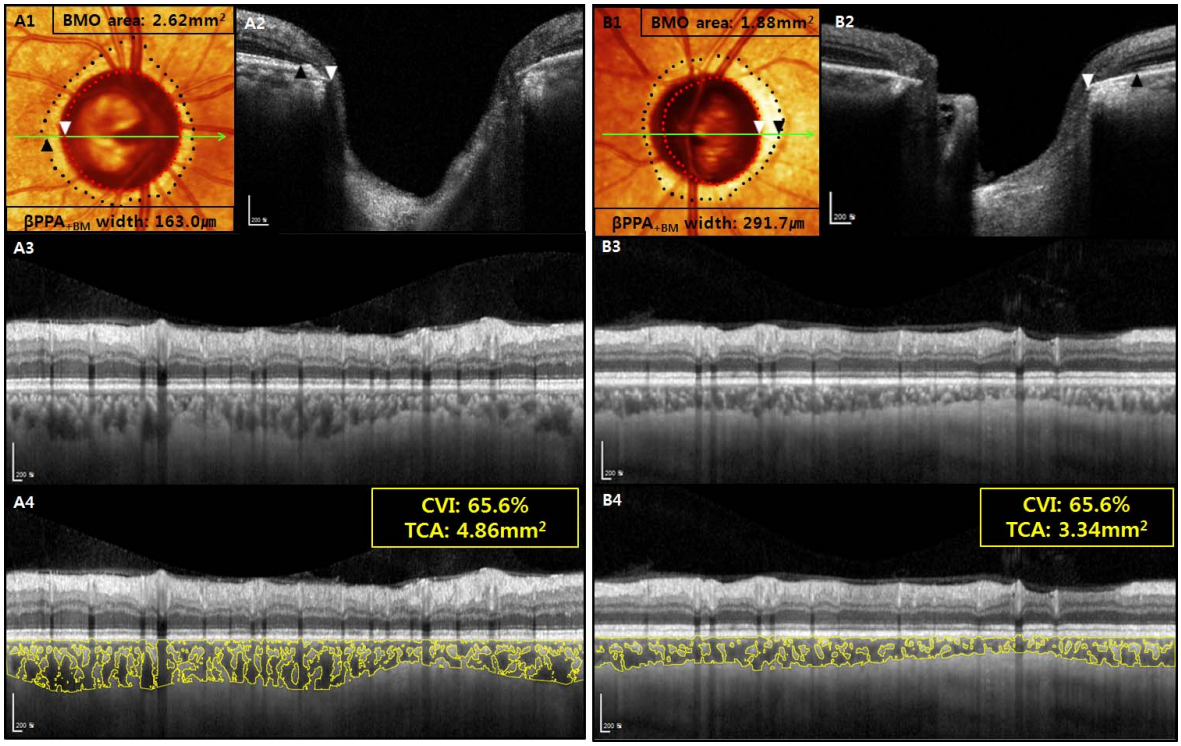

Figure 1. Primary open-angle glaucoma patients showing differing TCA with similar choroidal vascularity index (CVI) according to width of β-zone parapapillary atrophy with Bruch's membrane (βPPA_{+BM}) derived by SD-OCT. βPPA_{+BM} width was determined as the distance between the Bruch's membrane opening (BMO) (*red dots* and *white arrowheads*) and the retinal pigment epithelium tip (*black dots* and *black arrowheads*) on color-converted infrared fundus images (**A1**, **B1**) with lines indicating level of horizontal cross-sectional SD-OCT images (**A2**, **B2**). CVI was derived as a proportion of the choroidal vasculature (*yellow outlines*) against the TCA by image binarization of the 3.5-mm-sized radial circle on the SD-OCT scan (**A3-4**, **B3-4**). (**A**) Left eye of 55-year-old male (axial length AXL = 24.12 mm and BMO area = 2.62 mm^2) with βPPA_{+BM} width of 163.0 μm (**A1**, **A2**) had TCA of 4.86 mm^2 and CVI of 65.6% (**A3**, **A4**). (**B**) Right eye of 54-year-old male (AXL = 24.47 mm and BMO area = 1.88 mm^2) with larger βPPA_{+BM} width (291.7 μm) (**B1**, **B2**) had smaller TCA (3.34 mm^2) despite similar CVI (65.6%) (**B3**, **B4**).

available elsewhere.[2,3,17,20] Briefly, public domain software, Image J (version 1.47),[33] was used by one masked grader (N.K.) to perform segmentation and binarization of the scanned image.[20,34,35] Then, the image was converted to RGB (red, green, blue) color to allow the color-threshold tool to select the dark pixels.[17,20] The CVI was calculated by dividing the luminal area (LA), defined as the vascular area of the dark pixels of the choroid, by the total choroidal area (TCA), defined as the area between the RPE and the choroid scleral junction[20] (Figs. 1A3-4, 1B3-4).

Data Analysis

Univariate and multivariate regression analyses were performed to determine the factors associated with the width of βPPA_{+BM} and βPPA_{-BM}. Linear regression analysis was performed to assess the relationship of TCA with CVI and LA, respectively. A Bland-Altman plot was used to evaluate the interobserver agreement on determination of the widths of βPPA_{+BM}, and βPPA_{-BM} and JPCT. Interobserver agreement in determining the presence of the βPPA, βPPA_{+BM}, βPPA_{-BM}, MvD_P, and focal LC defect was assessed using the kappa coefficient.[36,37] All of the statistical analyses were performed with MedCalc (MedCalc, Inc., Mariakerke, Belgium). The α level (type I error) was set at 0.05.

Results

Among 182 eyes of 182 consecutive POAG patients who had been evaluated for eligibility, 22 were excluded for the following reasons: (1) poor-quality SD-OCT images (n = 5) and/or poor-quality OCT-A images (n = 6); (2) failure to reach interobserver consensus on determination of focal LC defect (n = 6) and/or MvD_P (n = 3); (3) unreliable VF results (n = 4). A total of 160 eyes of 160 subjects finally were included in the analysis. There was an overlap of 93 subjects between the present and previous studies.[20]

The 95% Bland-Altman limits of agreement between the measurements from the two observers were −2.64 to 1.70 for βPPA_{+BM} width, −4.75 to −0.57 for βPPA_{-BM} width, and −2.03 to 0.76 for JPCT. Interobserver agreement in determining the presence of the βPPA, βPPA_{-BM}, MvD_P, and focal LC defect was excellent (kappa = 0.90 for βPPA, kappa = 0.87 for βPPA_{-BM}, kappa = 0.84 for MvD_P, and kappa = 0.83 for focal LC defect).

The baseline characteristics of the subjects are provided in Table 1. The patients were aged 56.2 ± 14.4 years (range, 22–88 years). The VF mean deviation (MD) and pattern standard deviation (PSD) were −5.3 ± 4.0 dB (range, −20.7 to 1.2 dB) and 6.2 ± 3.7 dB (range, 1.7–14.8 dB), respectively. Ninety-two eyes (57.5%) had βPPA_{-BM}, while 68 eyes (42.5%) did not have βPPA_{-BM}. The βPPA_{+BM} and βPPA_{-BM} widths were 216.6 ± 107.6 mm (range, 41.7–645.2 mm) and 187.0 ± 233.9 mm (range, 0–1148.5 mm), respectively. The number of eyes with MvD_P was 89 (55.6%). JPCT, CVI, and TCA were 108.8 ± 39.4 μm (range, 39.2–276.2 μm), 61.8 ± 4.3% (range, 49.2–73.4%), and 3.6 ± 1.1 mm^2 (range, 1.4–6.4 mm^2), respectively.

The univariate and multivariate regression analyses of the association between the βPPA_{+BM} and clinical and ocular features are presented in Table 2. The univariate regression

Table 1. Demographics and Test Results of 160 Primary Open-Angle Glaucoma Patients

Variables	
Age, y	56.2 ± 14.4 (22 to 88)
Sex, male/female	81/79
Spherical equivalent, D	−2.6 ± 3.8 (−13.3 to 3.0)
Axial length, mm	25.0 ± 1.8 (21.4 to 29.8)
CCT, μm	537.3 ± 34.2 (462.0 to 647.0)
Self-reported history of diabetes, *n* (%)	13 (8.1)
Self-reported history of hypertension, *n* (%)	30 (18.8)
BIOP, mm Hg	17.3 ± 6.1 (9.0 to 47.0)
IOP, mm Hg	12.2 ± 2.6 (7.0 to 25.0)
Systolic BP, mm Hg	122.6 ± 14.9 (88.0 to 168.0)
Diastolic BP, mm Hg	74.0 ± 11.9 (50.0 to 110.0)
Mean ocular perfusion pressure, mm Hg	47.5 ± 8.5 (26.1 to 67.0)
Disc hemorrhage, *n* (%)	21 (13.1)
Visual field MD, dB	−5.3 ± 4.0 (−20.7 to 1.2)
Visual field PSD, dB	6.2 ± 3.7 (1.7 to 14.8)
BMO area, mm^2	2.4 ± 0.7 (1.3 to 6.4)
Focal lamina cribrosa defect, *n* (%)	59 (36.9)
Fovea–BMO angle, °	−7.0 ± 3.6 (−21.4 to 4.4)
Presence of the βPPA_{-BM}, *n* (%)	92 (57.5)
βPPA width, mm	403.5 ± 258.5 (79.9 to 1628.8)
βPPA_{+BM} width, mm	216.6 ± 107.6 (41.7 to 645.2)
βPPA_{-BM} width, mm	187.0 ± 233.9 (0 to 1148.5)
MvD_P, *n* (%)	89 (55.6)
Juxtapapillary choroidal thickness, μm	108.5 ± 39.4 (39.2 to 276.2)
Choroidal vascularity index, %	61.8 ± 4.3 (49.2 to 73.4)
Total choroidal area, mm^2	3.6 ± 1.1 (1.4 to 6.4)
Luminal area, mm^2	2.3 ± 0.8 (0.7 to 4.2)

Continuous variables are shown in mean ± standard deviation (range). BIOP, baseline intraocular pressure.

analysis revealed that larger βPPA_{+BM} was significantly associated with older age, thinner JPCT, smaller TCA, smaller LA, and lower CVI (all $P < 0.05$; Table 2). Sex, CCT, AXL, IOP at the scan time, baseline IOP, systolic and diastolic BPs, MOPP, diabetes, hypertension, DH, VF MD, VF PSD, focal LC defect, BM opening area, fovea–BM opening angle, and MvD_P were not associated with βPPA_{+BM} width ($P > 0.10$; Table 2). Because TCA and LA had high variance inflation factors, these two factors were included separately in the multivariate model to avoid multicollinearity. In the multivariate regression analysis with TCA included, older age ($P = 0.040$) and smaller TCA ($P = 0.023$) remained as significant factors associated with larger βPPA_{+BM}; in the multivariate regression analysis with LA included, older age ($P = 0.035$) and smaller LA ($P = 0.044$) remained as significant factors associated with larger βPPA_{+BM} (Table 2). For both multivariate regression analyses, JPCT and CVI were excluded ($P > 0.05$) (Fig. 1).

The univariate and multivariate regression analyses of the association between βPPA_{-BM} and the clinical and structural parameters are presented in Table 2. The univariate regression analysis revealed that larger βPPA_{-BM} was significantly associated with younger age, longer AXL, absence of hypertension, and larger BM opening area (all $P < 0.05$; Table 3). VF PSD ($P = 0.094$), larger fovea–BM opening angle ($P = 0.052$), and smaller LA ($P = 0.079$) were associated with larger βPPA_{-BM} with marginal significance (Table 3). Sex, CCT, IOP at the scan time, baseline IOP, systolic and diastolic BPs, MOPP, diabetes, DH, VF MD and PSD, focal LC defect, JPCT, TCA, CVI, and presence of MvD_P were not associated with βPPA_{-BM} ($P > 0.10$; Table 3) (Fig. 2). In the multivariate regression analysis, younger age, longer AXL, worse PSD, and larger BM opening area remained as significant factors associated with larger βPPA_{-BM} ($P < 0.05$; Table 3). Meanwhile, HT, fovea–BM opening angle, and LA were excluded in the multivariate analysis ($P < 0.10$; Table 3).

Figure 3 shows the relationship of TCA with LA and CVI. TCA had a significant correlation with both LA ($r = 0.991$) and CVI ($r = 0.698$) ($P < 0.05$).

Discussion

In the present study, the total area of the choroidal tissue and vasculature were quantified as TCA and LA, respectively, using the image binarization technique of SD-OCT. Furthermore, the percentage choroidal vessel density was quantified as CVI. This study found that CVI differed from TCA and LA in terms of their relationship with the PPA microstructure. Particularly, larger βPPA_{+BM} was significantly associated with smaller TCA and LA, but not with CVI. In addition, TCA was highly associated with LA ($r = 0.991$), and the two parameters showed high multicollinearity in assessing factors associated with βPPA_{+BM} width. These findings suggest that reduced choroidal vascularity is indirectly related with RPE atrophy, and may be an epiphenomenon of the choroidal thinning in glaucomatous eyes with βPPA_{+BM}.

Recent studies reported that reduced choroidal tissue was significantly associated with larger βPPA_{+BM}.[14,15] Possible explanations include atrophic degeneration and impaired microvasculature of the BM–RPE complex associated with reduced choroidal perfusion of adjacent areas and subsequent choroidal thinning.[14,15] However, such speculations need to be validated by direct measurement of the choroidal vasculature rather than by measurement of choroidal thickness as its surrogate. The current result concurs with a previous study in that reduced TCA was significantly associated with the extent of βPPA_{+BM} in a multivariate regression analysis. However, percentage CVI was not associated with βPPA_{+BM} width after adjusting for possible confounding factors including age, JPCT, and TCA. The clinical implications of these findings are not clear. Possible explanations include the hypothesis that βPPA_{+BM} width is an independent factor associated with the peripapillary choroidal area, but not with the choroidal vascularity outside βPPA. The influence of the atrophic change of the RPE–BM complex on the adjacent choroid possibly is not solely caused by vascular insufficiency but also owing to other mechanisms including developmentally thin choroidal tissue.[14] Rather, choroidal vascularity could be an epiphenomenon of choroidal thinning. Although the total area of choroidal vasculature was associated with the βPPA_{+BM} width ($r = -0.326$), it was also highly associated the TCA ($r = 0.911$) with high multicollinearity in assessing factors related with βPPA_{+BM} width. These findings support the notion that choroidal vasculature is indirectly associated with the RPE atrophy and may be mediated by the choroidal thinning. However, such speculations need to be confirmed by further experimental and clinical studies investigating the mechanisms of the relationship between choroidal vascularity and RPE/choroidal atrophy.

In this study, JPCT was excluded in the multivariate regression analysis for the βPPA_{+BM} width. This may be because the area of peripapillary choroidal tissue and vasculature had a stronger relationship with the βPPA_{+BM} width than did the JPCT. When multivariate regression analysis on the JPCT was performed using age, CCT, and βPPA width, but not CVI and TCA, as independent variables, JPCT was negatively associated with the βPPA_{+BM} width ($P = 0.049$) and

Table 2. Regression Analysis Testing Factors Associated Width of the βPPA With Bruch's Membrane, $n = 160$

	Univariate Model		Multivariate Model 1* TCA Included		Multivariate Model 2* LA Included	
Variables	**Beta (95% CI)**	***P* Value**	**Beta (95% CI)**	***P* Value**	**Beta (95% CI)**	***P* Value**
Age, per 1 y older	1.75 (0.61 to 2.90)	**0.003**	1.21 (0.06~2.36)	**0.040**	1.24 (0.09~2.40)	**0.035**
Female sex, versus male	16.38 (−17.59 to 50.35)	0.342				
CCT, per 1 μm thicker	−0.24 (−0.75 to 0.27)	0.357				
Axial length, per 1 mm longer	−3.66 (−13.46 to 6.14)	0.462				
IOP at the scan time, per 1 mm Hg higher	−0.21 (−6.77 to 6.35)	0.950				
Baseline IOP, per 1 mm Hg higher	−0.92 (−3.86 to 2.03)	0.539				
Systolic BP, per 1 mm Hg higher	−0.36 (−1.60 to 0.87)	0.562				
Diastolic BP, per 1 mm Hg higher	−0.72 (−2.27 to 0.83)	0.361				
Mean ocular perfusion pressure, per 1 mm Hg higher	−0.89 (−3.82 to 2.05)	0.550				
Diabetes, presence	−10.80 (−74.19 to 52.59)	0.737				
Hypertension, presence	8.19 (−35.80 to 52.18)	0.714				
Disc hemorrhage, presence	20.14 (−30.46 to 70.74)	0.433				
Visual field MD, per 1 dB worse	−0.50 (−4.85 to 3.85)	0.821				
Visual field PSD, per 1 dB worse	−2.67 (−7.31 to 1.98)	0.258				
Focal lamina cribrosa defect, presence	−21.84 (−57.06 to 13.39)	0.223				
BM opening area, per 1 mm^2 larger	16.73 (−7.48 to 40.95)	0.174				
Fovea–BM opening angle, per 1° larger	0.22 (−4.57 to 5.02)	0.927				
JPCT, per 1 μm thicker	−0.64 (−1.06 to −0.22)	**0.003**	0.17 (−0.43 to 0.76)	0.577	0.13 (−0.48 to 0.74)	0.673
TCA, per 1 mm^2 increase	−32.73 (−47.17 to −18.30)	**<0.001**	−28.37 (−52.82 to −3.93)	**0.023**		
LA, per 1 mm^2 increase	−44.20 (−64.19 to −24.21)	**<0.001**			−39.69 (−78.22 to −1.16)	**0.044**
CVI, per 1% increase	−6.95 (−10.81 to −3.08)	**<0.001**	−1.81 (−7.10 to 3.48)	0.500	−0.09 (−6.90 to 5.11)	0.767
MvD_P, presence	−24.00 (−58.12 to −10.12)	0.167				

Statistically significant values are shown in bold. CI, confidence interval.
* Adjusted for all variables with $P < 0.1$ in univariate regression model.

age ($P = 0.044$) (data not shown in Results). These results concur with those of the previous studies.[14,15]

The present result that TCA, LA, and CVI were not associated with βPPA_{-BM} width corresponds with a previous study reporting that JPCT was not associated with βPPA_{-BM}.[12] These findings imply that βPPA_{-BM}, which is known to be caused mainly by axial elongation, does not have any remarkable influence on peripapillary choroidal vascularity or tissue thickness.

CVI represents the density of vessels within a specified area of the choroid whereas LA represents the actual vascular area in the choroid. We consider that CVI is more suitable than LA for the main purpose of this study investigating the relationship between the choroidal vasculature and βPPA microstructure after minimizing influence of the choroidal tissue. There was a strong association between the LA and TCA ($r = 0.991$) compared with that between the CVI and TCA ($r = 0.698$) (Fig. 3). In addition, both TCA and LA are absolute values and CVI is a ratio of LA upon TCA. As TCA and LA are likely to be influenced by physiological changes including age, sex, and refractive errors,[17] we needed to look for the more stable index of choroidal function, and that is where CVI was invented. It is less influenced by TCA and by physiologic variables; hence we opted to use CVI over TCA or LA. Similarly, previous studies used a percentage vessel density calculated as the proportion of the measured area occupied by flowing blood vessels, not its absolute value, for assessing the vascularity of the superficial layer microvasculature.[38,39]

The present study has several limitations. First, the image binarization technique for the measurement of CVI has technical limitations including poor isolation of the choriocapillaris, the possibility of falsely high CVI measurement due to shadowing of the large superficial retinal vessels, and lack of adjustment of ocular magnification for the calculation of TCA.[20] However, these limitations can be at least partially addressed by the results showing that AXL was not associated with CVI or TCA in the univariate regression analysis, and also by a number of studies using the current image binarization technique for both normal subjects and various retinal diseases.[20] Second, this study is limited by its cross-sectional design and recruitment of patients from a hospital outpatient clinic, and therefore might not be adequate for representation of a general population. Third, it should be noted that the clinical disc margin has no consistent anatomic foundation[40,41]; this region falls inside the OCT-derived BMO, and is either bare sclera or border tissues of Elschnig or some combination of the two. This could lead to a variation of βPPA_{-BM} width.[40] However, we used infrared fundus images as an adjunct for the

Table 3. Regression Analysis Testing Factors Associated Width of the βPPA Without Bruch's Membrane, $n = 160$

	Univariate Model		Multivariate Model*	
Variables	**Beta (95% CI)**	***P* Value**	**Beta (95% CI)**	***P* Value**
Age, per 1 y older	−7.55 (−9.78 to −5.32)	**<0.001**	−3.87 (−6.22 to −1.53)	**0.001**
Female sex, versus male	−19.13 (−91.83 to 53.57)	0.604		
CCT, per 1 μm thicker	0.29 (−0.82 to 1.40)	0.607		
Axial length, per 1 mm longer	79.16 (64.29 to 94.03)	**<0.001**	46.30 (27.88 to 64.72)	**<0.001**
IOP at the scan time, per 1 mm Hg higher	−3.79 (−17.78 to 10.21)	0.594		
Baseline IOP, per 1 mm Hg higher	−2.41 (−8.87 to 4.05)	0.462		
Systolic BP, per 1 mm Hg higher	−0.53 (−3.17 to 2.11)	0.692		
Diastolic BP, per 1 mm Hg higher	0.33 (−3.00 to 3.65)	0.847		
Mean ocular perfusion pressure, per 1 mm Hg higher	0.84 (−5.24 to 6.93)	0.784		
Diabetes, presence	−63.29 (−197.82 to 71.23)	0.354		
Hypertension, presence	−123.80 (−215.63 to −32.00)	**0.009**	9.52 (−78.42 to 59.38)	0.785
Disc hemorrhage, presence	−41.07 (−149.18 to 67.04)	0.454		
Visual field MD, per 1 dB worse	−0.13 (−9.42 to 9.15)	0.977		
Visual field PSD, per 1 dB worse	8.43 (−1.44 to 18.30)	0.094	8.02 (1.21 to 14.84)	**0.022**
Focal lamina cribrosa defect, presence	5.02 (−70.57 to 80.61)	0.896		
BM opening area, per 1 mm^2 larger	180.06 (137.05 to 223.07)	**<0.001**	108.89 (66.51 to 151.27)	**<0.001**
Fovea-BM opening angle, per 1° larger	10.16 (−0.07 to 20.38)	0.052	−3.55 (−10.48 to 3.38)	0.313
JPCT, per 1 μm thicker	−0.12 (−1.05 to 0.80)	0.764		
TCA, per 1 mm^2 increase	−27.21 (−59.65 to 5.22)	0.100		
LA, per 1 mm^2 increase	−40.00 (−84.74 to 4.75)	0.079	−16.56 (−51.20 to 18.08)	0.346
CVI, per 1% increase	−5.49 (−14.02 to 3.04)	0.205		
MvD_P, presence	−55.27 (−128.07 to 17.54)	0.136		

Statistically significant values are shown in bold.
* Adjusted for all variables with $P < 0.1$ in univariate regression model.

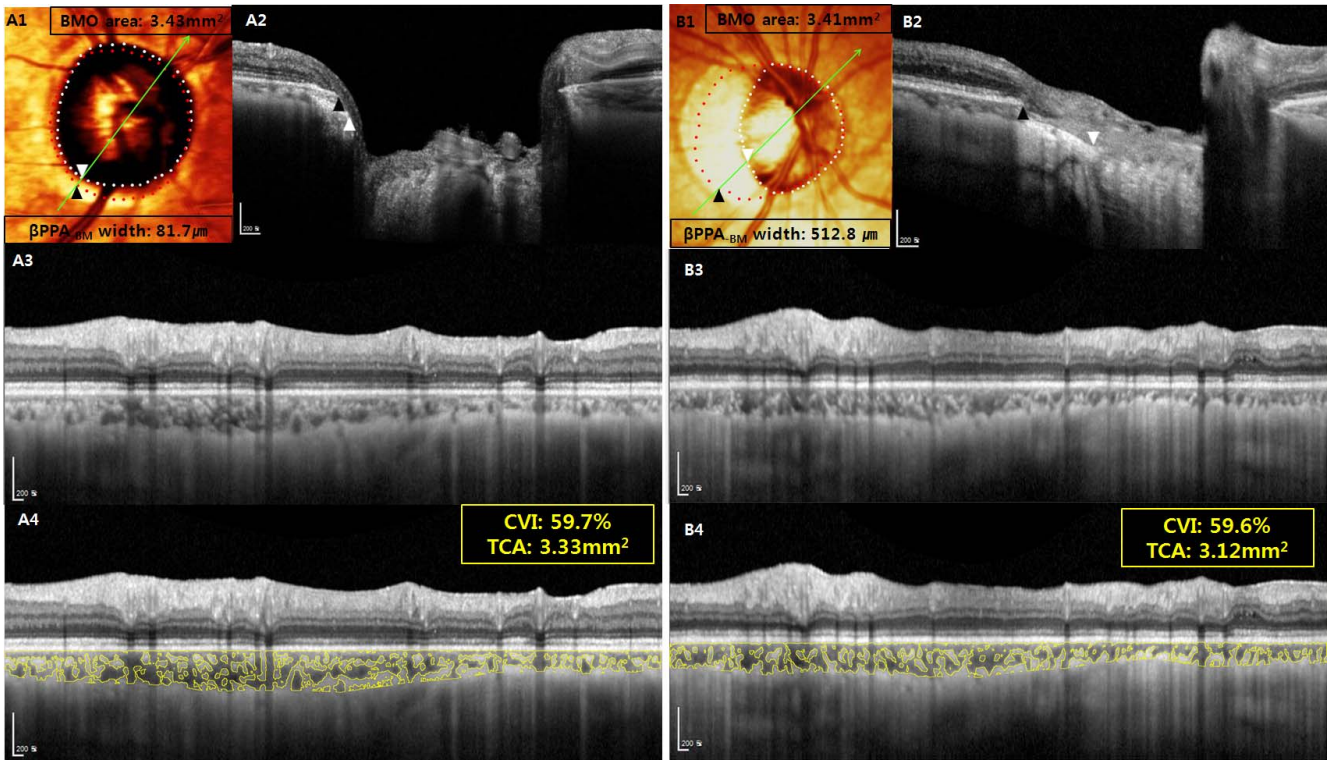

Figure 2. Primary open-angle glaucoma patients showing similar TCA and choroidal vascularity index (CVI) with differing β-zone parapapillary atrophy without Bruch's membrane (βPPA_{-BM}) width. βPPA_{-BM} width was determined as the distance between Bruch's membrane opening (BMO) (*red dots* and *black arrowheads*) and the clinical disc margin (*white dots* and *white arrowheads*) on color-converted infrared fundus images (**A1**, **B1**) with lines indicating a level of horizontal cross-sectional SD-OCT images (**A2**, **B2**). CVI was derived as a proportion of the choroidal vasculature (*yellow outlines*) against the TCA by image binarization of the 3.5-mm-sized radial circle on the SD-OCT scan (**A3-4**, **B3-4**). (**A**) Right eye of 60-year-old female (axial length = 24.49 mm and BMO area = 3.43 mm^2) with βPPA_{-BM} width of 81.μm (**A1**, **A2**) had TCA of 3.33 mm^2 and CVI of 59.7% (**A3**, **A4**). (**B**) Right eye of 60-year-old male (AXL = 28.66 mm and BMO area = 3.41 mm^2) with larger βPPA_{-BM} width (512.8 μm) (**B1**, **B2**) had similar TCA (3.12 mm^2) and CVI (59.6%) (**B3**, **B4**).

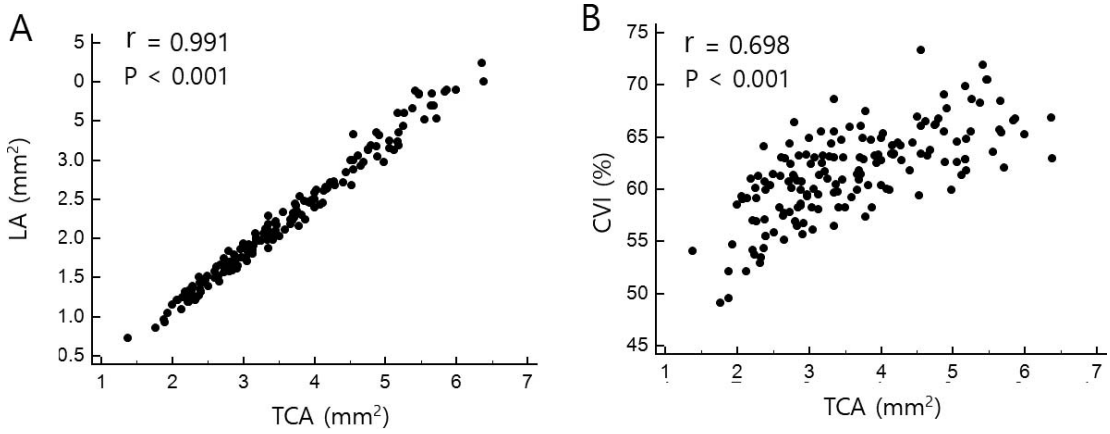

FIGURE 3. Scatter plots showing the association between the TCA and LA (**A**) and between the TCA and choroidal vascularity index (CVI) (**B**), respectively. TCA was significantly associated with both LA ($r = 0.991$) and CVI ($r = 0.698$) ($P < 0.05$).

clinical disc margin, and in that way, we found a good interobserver agreement for measurement of βPPA_{-BM}. Recently, the anterior scleral canal opening (ASCO) was introduced as a stable anatomic landmark, although it is often challenging to segment ASCO accurately.[9,42] As OCT visualization and segmentation improves, segmenting the ASCO will be helpful in further clarifying the anatomy of the parapapillary ONH structure. Finally, this study quantified the choroidal vasculature, but not the blood flow itself. Theoretically, it is possible that increased velocity of the blood flow may compensate for the decreased choroidal vascularity. Therefore, reduced choroidal vascularity should not be interpreted as the decreased choroidal perfusion in glaucomatous eyes.

In conclusion, larger βPPA_{+BM} was significantly associated with the smaller total area of the peripapillary choroidal tissue and vasculature, but not with peripapillary choroidal vessel density outside the βPPA, as measured by the image binarization technique of SD-OCT. In addition, the total area of the choroidal tissue and vasculature were highly associated. These findings suggest that previously suggested common mechanism between the RPE and choroidal atrophy may not be mediated by the impaired choroidal perfusion in glaucomatous eyes. Further longitudinal studies on the temporal relationship between the RPE atrophy and choroidal atrophy are needed.

Acknowledgments

The authors thank Hae Rang Kim, MD, for her data acquisition.

Disclosure: **M.H. Suh**, None; **J.W. Park**, None; **N. Khandelwal**, None; **R. Agrawal**, None

References

1. Alm A, Bill A. Ocular and optic nerve blood flow at normal and increased intraocular pressures in monkeys (Macaca irus): a study with radioactively labelled microspheres including flow determinations in brain and some other tissues. *Exp Eye Res*. 1973;15:15–29.
2. Agrawal R, Salman M, Tan KA, et al. Choroidal vascularity index (CVI)—a novel optical coherence tomography parameter for monitoring patients with panuveitis? *PLoS One*. 2016; 11:e0146344.
3. Wei X, Ting DSW, Ng WY, Khandelwal N, Agrawal R, Cheung CMG. Choroidal vascularity index - a novel optical coherence tomography based parameter in patients with exudative age-related macular degeneration. *Retina*. 2017;37:1120–1125.
4. Tan KA, Laude A, Yip V, Loo E, Wong EP, Agrawal R. Choroidal vascularity index – a novel optical coherence tomography parameter for disease monitoring in diabetes mellitus? *Acta Ophthalmol*. 2016;94:e612–e616.
5. Agrawal R, Chhablani J, Tan K-A, Shah S, Sarvaiya C, Banker A. Choroidal vascularity index in central serous chorioretinopathy. *Retina*. 2016;36:1646–1651.
6. Anderson DR, Braverman S. Reevaluation of the optic disk vasculature. *Am J Ophthalmol*. 1976;82:165–174.
7. Lieberman MF, Maumenee AE, Green WR. Histologic studies of the vasculature of the anterior optic nerve. *Am J Ophthalmol*. 1976;82:405–423.
8. Onda E, Cioffi GA, Bacon DR, Van Buskirk EM. Microvasculature of the human optic nerve. *Am J Ophthalmol*. 1995;120: 92–102.
9. Yang H, Luo H, Gardiner SK, et al. Factors influencing optical coherence tomography peripapillary choroidal thickness: a multicenter study. *Invest Ophthalmol Vis Sci*. 2019:60:795–806.
10. Sigal IA, Yang H, Roberts MD, et al. IOP-induced lamina cribrosa deformation and scleral canal expansion: independent or related? *Invest Ophthalmol Vis Sci*. 2011;52:9023–9032.
11. Hayreh SS, Revie IH, Edwards J. Vasogenic origin of visual field defects and optic nerve changes in glaucoma. *Br J Ophthalmol*. 1970;54:461–472.
12. O'Brart DP, de Souza Lima M, Bartsch DU, Freeman W, Weinreb RN. Indocyanine green angiography of the peripapillary region in glaucomatous eyes by confocal scanning laser ophthalmoscopy. *Am J Ophthalmol*. 1997;123:657–666.
13. Spraul CW, Lang GE, Lang GK, Grossniklaus HE. Morphometric changes of the choriocapillaris and the choroidal vasculature in eyes with advanced glaucomatous changes. *Vision Res*. 2002;42:923–932.
14. Sullivan-Mee M, Patel NB, Pensyl D, Qualls C. Relationship between juxtapapillary choroidal volume and beta-zone parapapillary atrophy in eyes with and without primary open-angle glaucoma. *Am J Ophthalmol*. 2015;160:637–647.
15. Lee SH, Lee EJ, Kim TW. Topographic correlation between juxtapapillary choroidal thickness and microstructure of parapapillary atrophy. *Ophthalmology*. 2016;123:1965–1973.
16. Lee KM, Lee EJ, Kim TW. Juxtapapillary choroid is thinner in normal-tension glaucoma than in healthy eyes. *Acta Ophthalmol*. 2016;94:e697–e708.
17. Agrawal R, Gupta P, Tan KA, Cheung CMG, Wong TY, Cheng CY. Choroidal vascularity index as a measure of vascular status

of the choroid: measurements in healthy eyes from a population-based study. *Sci Rep*. 2016;6:1–9.

18. Agrawal R, Li LKH, Nakhate V, Khandelwal N, Mahendradas P. Choroidal vascularity index in Vogt-Koyanagi-Harada disease: an EDI-OCT derived tool for monitoring disease progression. *Trans Vis Sci Tech*. 2016;5(4):7.
19. Ng WY, Ting DSW, Agrawal R, et al. Choroidal structural changes in myopic choroidal neovascularization after treatment with antivascular endothelial growth factor over 1 year. *Invest Ophthalmol Vis Sci*. 2016;57:4933–4939.
20. Park JW, Suh MH, Agrawal R, Khandelwal N. Peripapillary choroidal vascularity index in glaucoma-a comparison between spectral-domain OCT and OCT angiography. *Invest Ophthalmol Vis Sci*. 2018;59:3694–3701.
21. Suh MH, Park JW, Kim HR. Association between the deep-layer microvasculature dropout and the visual field damage in glaucoma. *J Glaucoma*. 2018;27:543–551.
22. Suh MH, Zangwill LM, Manalastas PIC, et al. Deep retinal layer microvasculature dropout detected by the optical coherence tomography angiography in glaucoma. *Ophthalmology*. 2016;123:2509–2518.
23. Park H-YL, Lee N-Y, Shin H-Y, Park CK. Analysis of macular and peripapillary choroidal thickness in glaucoma patients by enhanced depth imaging optical coherence tomography. *J Glaucoma*. 2014;23:225–231.
24. Suh MH, Zangwill LM, Manalastas PIC, et al. Deep-layer microvasculature dropout by optical coherence tomography angiography and microstructure of parapapillary atrophy. *Invest Ophthalmol Vis Sci*. 2018;59:1995–2004.
25. Suh MH, Zangwill LM, Manalastas PIC, et al. Optical coherence tomography angiography vessel density in glaucomatous eyes with focal lamina cribrosa defects. *Ophthalmology*. 2016;123:2309–2317.
26. Kiumehr S, Park SC, Dorairaj S, et al. In vivo evaluation of focal lamina cribrosa defects in glaucoma. *Arch Ophthalmol*. 2012;130:552–559.
27. Park SC, Hsu AT, Su D, et al. Factors associated with focal lamina cribrosa defects in glaucoma. *Invest Ophthalmol Vis Sci*. 2013;54:8401–8407.
28. Kim M, Kim T-W, Weinreb RN, Lee EJ. Differentiation of parapapillary atrophy using spectral-domain optical coherence tomography. *Ophthalmology*. 2013;120:1790–1797.
29. Dai Y, Jonas JB, Huang H, Wang M, Sun X. Microstructure of parapapillary atrophy: beta zone and gamma zone. *Invest Ophthalmol Vis Sci*. 2013;54:2013–2018.
30. Yamada H, Akagi T, Nakanishi H, et al. Microstructure of peripapillary atrophy and subsequent visual field progression in treated primary open-angle glaucoma. *Ophthalmology*. 2016;123:542–551.
31. Kim YW, Lee EJ, Kim TW, Kim M, Kim H. Microstructure of β-zone parapapillary atrophy and rate of retinal nerve fiber layer thinning in primary open-angle glaucoma. *Ophthalmology*. 2014;121:1341–1349.
32. Jonas JB, Jonas SB, Jonas RA, et al. Parapapillary atrophy: histological gamma zone and delta zone. *PLoS One*. 2012;7:e47237.
33. Schneider CA, Rasband WS, Eliceiri KW. NIH Image to ImageJ: 25 years of image analysis. *Nat Methods*. 2012;9:671–675.
34. Sonoda S, Sakamoto T, Yamashita T, et al. Choroidal structure in normal eyes and after photodynamic therapy determined by binarization of optical coherence tomographic images. *Invest Ophthalmol Vis Sci*. 2014;55:3893–3898.
35. Sonoda S, Sakamoto T, Yamashita T, et al. Luminal and stromal areas of choroid determined by binarization method of optical coherence tomographic images. *Am J Ophthalmol*. 2015;159:1123–1131.
36. Cohen J. Weighted kappa: nominal scale agreement with provision for scaled disagreement or partial credit. *Psychol Bull*. 1968;70:213–220.
37. Landis JR, Koch GG. An application of hierarchical kappa-type statistics in the assessment of majority agreement among multiple observers. *Biometrics*. 1977;33:363–374.
38. Yarmohammadi A, Zangwill LM, Diniz-Filho A, et al. OCT angiography vessel density in healthy, glaucoma suspects, and glaucoma. *Invest Ophthalmol Vis Sci*. 2016;57:OCT451–OCT459.
39. Suh MH, Zangwill LM, Manalastas PI, et al. Optical coherence tomography angiography vessel density in glaucomatous eyes with focal lamina cribrosa defects. *Ophthalmology*. 2016;123:2309–2317.
40. Hong SW, Koenigsman H, Ren R, et al. Glaucoma specialist optic disc margin, rim margin and rim width discordance in glaucoma and glaucoma suspect eyes. *Am J Ophthalmol*. 2018;192:65–76.
41. Chauhan BC, Burgoyne CF. From clinical examination of the optic disc to clinical assessment of the optic nerve head: a paradigm change. *Am J Ophthalmol*. 2013;156:218–227.
42. Hong S, Yang H, Gardiner SK, et al. OCT-detected optic nerve head neural canal direction, obliqueness and minimum cross-sectional area in healthy eyes [published online ahead of print May 13, 2019]. *Am J Ophthalmol*. https://doi.org/10.1016/j.ajo.2019.05.009.

Investigative Ophthalmology & Visual Science